DRAFT VERSION APRIL 10, 2014
Preprint typeset using LaTeX style emulateapj v. 5/2/11

arXiv:1404.2281v1 [astro-ph.GA] 8 Apr 2014

PROBING ASYMMETRIC STRUCTURES IN THE OUTSKIRTS OF GALAXIES

ZHANG ZHENG WEN[1,2], XIAN ZHONG ZHENG[1] AND FANG XIA AN[1]

Draft version April 10, 2014

ABSTRACT

Upcoming large imaging surveys will allow detailed studies of the structure and morphology of galaxies aimed at addressing how galaxies form and evolve. Computational approaches are needed to characterize their morphologies over large samples. We introduce an automatic method to quantify the outer structure of galaxies. The key to our approach is the division of a galaxy image into two sections delineated by the isophote which encloses half the total brightness of the galaxy. We call the central section the inner half-flux region (IHR) and the outer section the outer half-flux region (OHR). From this division, we derive two parameters: $A_{\rm o}$, which measures the asymmetry of the OHR, and $D_{\rm o}$, which measures the deviation of the intensity weighted centroid of the OHR from that of the IHR relative to the effective radius. We derive the two parameters from *HST*/ACS z_{850}-band images for a sample of 764 galaxies with $z_{850} < 22$ mag and $0.35 < z < 0.9$ selected from GEMS and GOODS-South surveys. We show that the sample galaxies having strong asymmetric structures, in particular tidal tails, are well-separated from those with regular morphologies in the $A_{\rm o}$-$D_{\rm o}$ space. Meanwhile, the widely used *CAS* and Gini-M_{20} methods turn out to be insensitive to such morphological features. We stress that the $A_{\rm o}$-$D_{\rm o}$ method is an efficient way to select galaxies with significant asymmetric features like tidal tails and study galaxy mergers in the dynamical phase traced by these delicate features.

Subject headings: galaxies: interactions — galaxies: fundamental parameters — galaxies: peculiar — galaxies: structure

1. INTRODUCTION

Major mergers between galaxies of comparable mass are expected to occur frequently in hierarchical models of galaxy formation and evolution (e.g., White & Rees 1978; Lacey & Cole 1993). Galaxy merging may be a crucial process that regulates galaxy mass assembly, galaxy morphology reshaping, growth of supermassive black holes, and enhancement of star formation (e.g., Barnes & Hernquist 1992; Sanders & Mirabel 1996; Springel et al. 2005; Hopkins et al. 2008, 2010; Bundy et al. 2009; Conselice 2014). Measuring the galaxy merger rate over cosmic time is thus a central task in determining the importance of the merging process relative to that of other physical processes (e.g., feedback and gas accretion) to driving galaxy evolution.

Much effort has been made to measure galaxy merger rate. Interacting or merging galaxies are rare ($\sim$2%) in the local universe (Athanassoula & Bosma 1985; Patton et al. 1997; Xu et al. 2004; Patton & Atfield 2008; Domingue et al. 2009), but they become more numerous at higher redshifts. However, the measurements of the merger rate are inconsistent with each other and are still under debate. While strong evolution characterized by $(1+z)^{3-6}$ was often reported (Le Fèvre et al. 2000; Patton et al. 2002; Conselice et al. 2003; Cassata et al. 2005; Kampczyk et al. 2007; Kartaltepe et al. 2007; Conselice et al. 2009; Jogee et al. 2009; Xu et al. 2010; Lotz et al. 2011), mild evolution following $\sim (1+z)^{0.5}$ or even no evolution was obtained by other studies (Carlberg et al. 2000; Bundy et al. 2004; Lin et al. 2008; Robaina et al. 2010; Man et al. 2012). The controversy is likely caused by large uncertainties in current observational techniques adopted for merger identification (see Lotz et al. 2008 for more details).

[1] Purple Mountain Observatory, Chinese Academy of Sciences, 2 West Beijing Road, Nanjing, 210008, China
[2] University of Chinese Academy of Sciences, 19A Yuquan Road Beijing, China

Disturbed morphology is mostly used as the probe of a merger. The violent tidal forces between merging galaxies can destroy galaxy structures and produce tidal features. For instance, extended tidal tails can be created when the mergers involve a disk galaxy (Toomre & Toomre 1972; Wright 1972; Barnes & Hernquist 1992; Mihos 2004). The characteristics of the tidal tails in turn disclose key properties of the parent galaxies such as kinematics, mass ratio, and orbital parameters (Duc 2013; Duc & Renaud 2013). A long tidal tail is usually seen as evidence for a merger between disk galaxies (e.g., Elmegreen et al. 2007; Bridge et al. 2010). Resolving specific features from mergers helps to provide information on the frequency of mergers, a better understanding of the merger time scale, and a complete census of various types of mergers over cosmic time. It further delivers insights on evolutionary pathways for different galaxy populations. This will be possible with upcoming deep imaging surveys over large areas (e.g., Euclid, Amendola et al. 2013). Computational approaches are keenly needed to detect the specific features tracing given types of mergers.

Non-parametric methods *CAS* (Conselice et al. 2000; Conselice 2003) and Gini-M_{20} (Lotz et al. 2004) are widely used for merger selection. *CAS* selects mergers mainly according to their morphological asymmetry, but fails to pick up those with weaker asymmetry in morphology (e.g., double-nucleus). The Gini coefficient and M_{20} parameters measure the relative distribution of pixel fluxes and spatial light concentration of a galaxy, respectively. Mergers and regular galaxies are globally separated in the Gini-M_{20} space. This method favors to select mergers that are in their first pass or the final stage (Lotz et al. 2008, 2010a,b). Neither *CAS* nor Gini-M_{20} provides a complete selection for major mergers (Kampczyk et al. 2007; Scarlata et al. 2007; Jogee et al. 2009; Kartaltepe et al. 2010). This is in part because the parameters adopted in the two methods are flux weighted. These parameters are largely determined by the light distribution of the bright section of a galaxy, and are insensitive to the tidal

features with lower surface brightness in the outskirts of the galaxy.

In this paper, we present a new approach to quantifying the structure of the outskirts of a galaxy, aimed at searching for tidal tails. Two parameters are introduced to accomplish this. In Section 2 we describe how to measure the two parameters. In Section 3, we verify our method using a visually classified sample of galaxies. Finally, we compare our method with *CAS* and Gini-M_{20} in Section 4. Throughout this paper, we assume $H_0 = 70\,\mathrm{km\,s^{-1}\,Mpc^{-1}}$, $\Omega_\Lambda = 0.7$ and $\Omega_\mathrm{m} = 0.3$.

2. METHODOLOGY

2.1. *Galaxy Division*

We divide the image of a galaxy into two sections split by the isophote which encloses half the total light of the galaxy. The inner section, named as the inner half-flux region (IHR), usually encloses a smaller area with a higher surface brightness than the outer section, named as the outer half-flux region (OHR). In practice, the IHR is identified first, and the rest of the galaxy is presumed to occupy the OHR. If the galaxy is regular in morphology, the two sections can be simply separated by the isophote which contains half the total light. If a galaxy does not have a single, clear core, but has double or even multiple comparable components, then we fix the center at the brightest component, and find the half-light isophote around this point.

We develop a technique to deal with image pixels and identify the brightest group of contiguous pixels as the brightest component in a galaxy image. The software tool SExtractor (Bertin & Arnouts 1996) is used to detect pixels that a galaxy covers in the background-subtracted image (see Section 3.3 for details). These pixels are sorted in descending order of flux. The pixels with highest fluxes are selected, yielding f, a ratio of the integrated flux to the total. More pixels within the galaxy will be included if a higher f is set. Starting from f=0.5, the selected pixels may spread into two or more discrete groups of contiguous pixels for galaxies with complex light distribution (e.g., late-type spirals with giant clumps). These discrete groups of pixels are then individually examined to obtain their integrated fluxes. By increasing f, each group is expected to contain more contiguous pixels and thus a higher fraction of the total flux. The brightest group with a sum of fluxes higher than 25% of the total is chosen to calculate a flux-weighted centroid. This position is taken as the center for isophotal fitting to the galaxy image. For a galaxy with smooth light distribution usually satisfying a Sérsic function, the selected pixels make up one group, which is indeed the IHR when $f = 0.5$. For a merging system with two nuclei, the brighter one will be selected. The factor of 25% is decided by this selection.

With the center fixed, elliptical isophotes are fitted to the galaxy image. Following the algorithms given in SExtractor, the ellipticity and position angle of an isophote are determined by the maximum and minimum spatial dispersion of the enclosed pixels by the real isophote. The ellipse containing 50% of the total flux is taken as the boundary for the IHR. And the pixels out of the isophote make up the OHR. Figure 1 demonstrates the separation between the IHR and OHR for two representative galaxies.

2.2. *Outer asymmetry*

The asymmetry parameter (A) is often used to quantify the morphological disturbance of a galaxy (Abraham et al. 1996; Conselice et al. 2000; Conselice 2003). It is calculated as the sum of the absolute residuals of the galaxy image subtracting itself rotated by 180° around its center. The rotation center is determined iteratively in order to minimize the asymmetry. We define outer asymmetry, A_o, as the asymmetry of the OHR of a galaxy following

$$A_\mathrm{o} = \frac{\sum |I_\mathrm{o} - I_\mathrm{o}^{180^\circ}|}{\sum I_\mathrm{o}} - \frac{\sum |B_\mathrm{o} - B_\mathrm{o}^{180^\circ}|}{\sum I_\mathrm{o}}, \qquad (1)$$

where I_o is flux distribution of the OHR and $I_\mathrm{o}^{180^\circ}$ represents the 180°-rotated I_o. In the same way, B_o is a patch in the background with the same shape as I_o. Again, $B_\mathrm{o}^{180^\circ}$ is the 180°-rotated B_o.

The rotation center is critical to the estimation of the asymmetry parameter. For very nearby galaxies, a small shift for the center would cause a significant change in the estimated asymmetry. For distant galaxies, determining a rotation center becomes less complicated because of decreasing resolution (Conselice et al. 2000). We thus adopt the centroid of the OHR as the rotation center when estimating A_o.

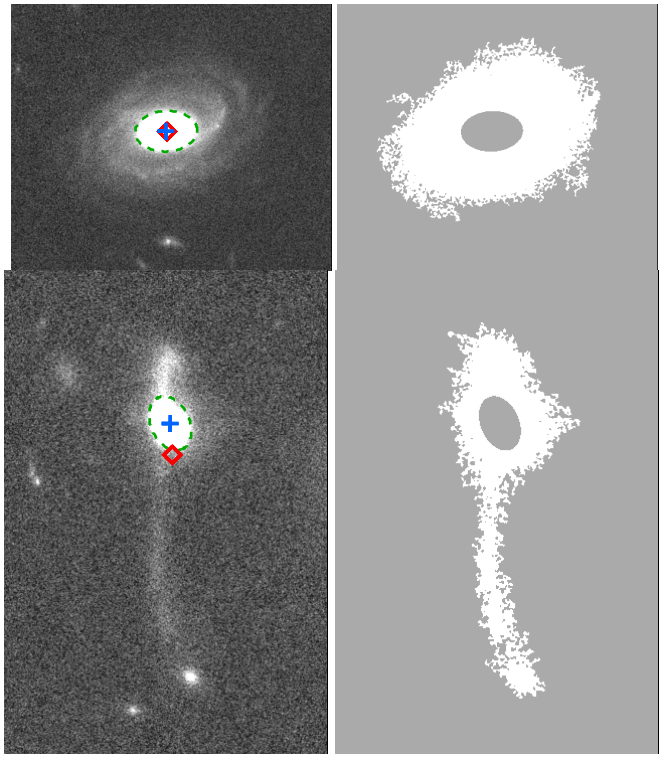

FIG. 1.— *HST*/ACS z_{850}-band images (left) and segmentation maps (right) for a typical spiral galaxy at $z = 0.47$ (top) and a merger with tidal tail at $z = 0.58$ (bottom). The ellipses (dashed lines) mark the IHR. The blue crosses and red diamonds give the centroids of the IHR and OHR of each galaxy, respectively.

2.3. *centroid deviation*

The centroid deviation parameter, D_o, measures the deviation (or offset) between centroids of the IHR and OHR of a galaxy. The centroid is determined by

$$x_\mathrm{cen} = \frac{\sum\limits_{i\in S} f_i\, x_i}{\sum\limits_{i\in S} f_i} \quad \text{and} \quad y_\mathrm{cen} = \frac{\sum\limits_{i\in S} f_i\, y_i}{\sum\limits_{i\in S} f_i}, \qquad (2)$$

where x_i and y_i define the position of pixel i in the galaxy image and f_i is flux of the pixel. The centroid deviation is calculated using the formula

$$D_o = \frac{\sqrt{(x_o - x_c)^2 + (y_o - y_c)^2}}{R_e}, \quad (3)$$

where (x_c,y_c) and (x_o,y_o) refer to the centroids of the IHR and OHR, respectively. The effective radius of the galaxy, R_e, is used for normalization. Here R_e is estimated using $R_e = \sqrt{n_c/\pi}$, where n_c is pixel count of the IHR.

For regular galaxies with symmetric morphologies, the IHR and OHR share nearly the same centroid, yielding a centroid deviation near zero. For merging galaxies with tidal tails, however, the centroid deviation becomes rather large, as shown in Figure 1. Similarly, the merging galaxies tend to have higher A_o than the regular galaxies. Therefore, galaxies with asymmetric structures are expected to be away from the regular galaxies in the diagram of A_o versus D_o. We test this A_o-D_o method using a sample of galaxies with high-resolution images from the Hubble Space Telescope (*HST*).

3. VERIFYING THE A_O-D_O METHOD

3.1. *Galaxy sample*

The extended Chandra Deep Field South (ECDFS) is one of the cosmic fields with the deepest multi-wavelength data over an area of $30' \times 30'$, including *HST*/ACS imaging data from the GEMS (Rix et al. 2004) and the GOODS-S surveys (Giavalisco et al. 2004), the survey catalog (Caldwell et al. 2008), photometry and photometric redshifts from the Multiwavelength Survey by Yale-Chile (MUSYC; Cardamone et al. 2010), and the stellar mass catalog from the COMBO-17 survey (Borch et al. 2006). The best-fit models of two-dimensional Sérsic profile derived from *HST* images are available for GEMS galaxies (Häussler et al. 2007). We use these data to select a sample of galaxies and test our method for quantifying morphologies of the OHRs.

We focus on massive galaxies that enable strong tidal features to be produced in the merging process and detectable at high-z. We derive morphological parameters from *HST*/ACS images in the z_{850} band, which corresponds to the rest-frame B to V in the redshift range $0.35 < z < 0.9$. In total, 825 galaxies are selected with stellar mass $\log(M/M_\odot) \geq 10.5$ and $0.35 < z < 0.9$ over the 800 square arcminutes area covered by *HST* observations. Of them, 32 objects are too compact to be resolved in morphology; and 29 objects are located at image edges. Finally, 764 galaxies are selected to compose a mass-complete sample for our morphological investigation. The sample galaxies are mostly with z_{850}-band magnitude $\sim 20-22$, compared to the $5\,\sigma$ depth of $z_{850} = 27.1$ mag.

The Sérsic index (n) is often used as a morphology indicator (e.g., n <2.5 for disk galaxies). However, the two-dimensional structural fitting ignores irregular structures that are crucial to identifying galaxy mergers, although the Sérsic models are good proxies for regular galaxies. Visual examination is still an efficient way to ascertain the tidal features. Our A_o-D_o method lacks sensitivity to distinguish galaxies with regular morphologies. We therefore adopt seven morphological types optimized for verifying the A_o-D_o method, including spheroids (E, S0), early disks (Sa-b), late disks (Sc-d), edge-on disks, irregulars/minor mergers, major mergers without tidal tail, and major mergers with tidal tails. The morphological classification was independently carried out by all three co-authors. As a result, the 764 galaxies in our sample are classified into 440, 57, 57, 27, 108, 60 and 15 from the first to the last class, respectively. We are interested in the latter three morphological classes, in particular major mergers with tidal tails. We note that tidal tails with a size of tens of kpcs at intermediate redshifts can be resolved with *HST*/ACS imaging. We explain in detail how to recognize a tidal feature as a tidal tail.

3.2. *The properties of tidal tails*

The visual investigation by Elmegreen et al. (2007) revealed that the host merging galaxies of tidal tails in ECDFS can be divided into four morphological types: diffuse, antennae, M51 and shrimp. Figure 2 shows *HST* images of merging galaxies with tidal tails selected from the ECDFS field.

The diffuse-type galaxies refer to those with diffuse arc-like or tail-like intergalactic structures (e.g., Kawata et al. 2006). Such tidal structures tend to have red color and smooth light profile, suggesting that they are tidal debris of early-type galaxies with little gas through dry mergers (e.g., the top-right panel in Figure 2).

The antennae-type galaxies have disturbed merger cores and extended tidal tails. They are most likely formed by major mergers between disk galaxies (e.g., Toomre & Toomre 1972). The visible timescale for tidal tails can be a few hundred Myrs (Conselice 2009) up to a few Gyrs (Hibbard & Mihos 1995). About half the merging galaxies with tidal tails shown in Figure 2 are antennae-type (e.g. ID 7357, 44488, 45115, 57896). Tidal dwarf galaxies can be formed in these tails, being a result of local gravitational instabilities of the gas component (Elmegreen et al. 1993; Bournaud & Duc 2006; Wetzstein et al. 2007) or at the tip of a tidal tail regulated by the accumulation and collapse of massive gaseous condensations (Duc et al. 2004). The presence of long tidal tails or tidal dwarfs dramatically increases A_o and D_o (see Section 3.3).

The M51-type galaxies are mergers at their early stages and the stellar bridge connecting one galaxy to the another is still seen. The galaxies of this type are rare probably because of the short timescale to be detected (several Myrs; Bournaud & Duc 2006). Shown in Figure 2, 11072 is a pair of galaxies of comparable z_{850}-band luminosity. The system has just undergone its first pericenter passage with a weak tidal bridge. A tail-like structure is seen with color $V_{606} - z_{850} = 1.28$, similar to the color of the central components ($V_{606} - z_{850} = 1.33$). No stellar clump is found on the tidal tail.

Finally, shrimp-type galaxies are characterized by a highly warped, dominant arm or tail and have no well-defined central nucleus. This type of merger is not included in Figure 2.

3.3. *The A_o-D_o classification*

Using *HST* images, we calculate outer asymmetry A_o and centroid deviation D_o for our sample of 764 galaxies. We run SExtractor to create a segmentation map for every galaxy. The segmentation map is an image with the same size as the scientific image where objects and their boundaries are determined. The total flux of a galaxy is then defined as the light contained in the pixels within its boundary. A detection threshold of $0.8\,\sigma_{bkg}$ above background is chosen. Here σ_{bkg} is the *RMS* of background noise. Other configuration parameters are set following Caldwell et al. (2008) for the GEMS catalog. This threshold is lower than usual settings (e.g., $1.65\,\sigma_{bkg}$, Caldwell et al. 2008) for source detection, aimed at

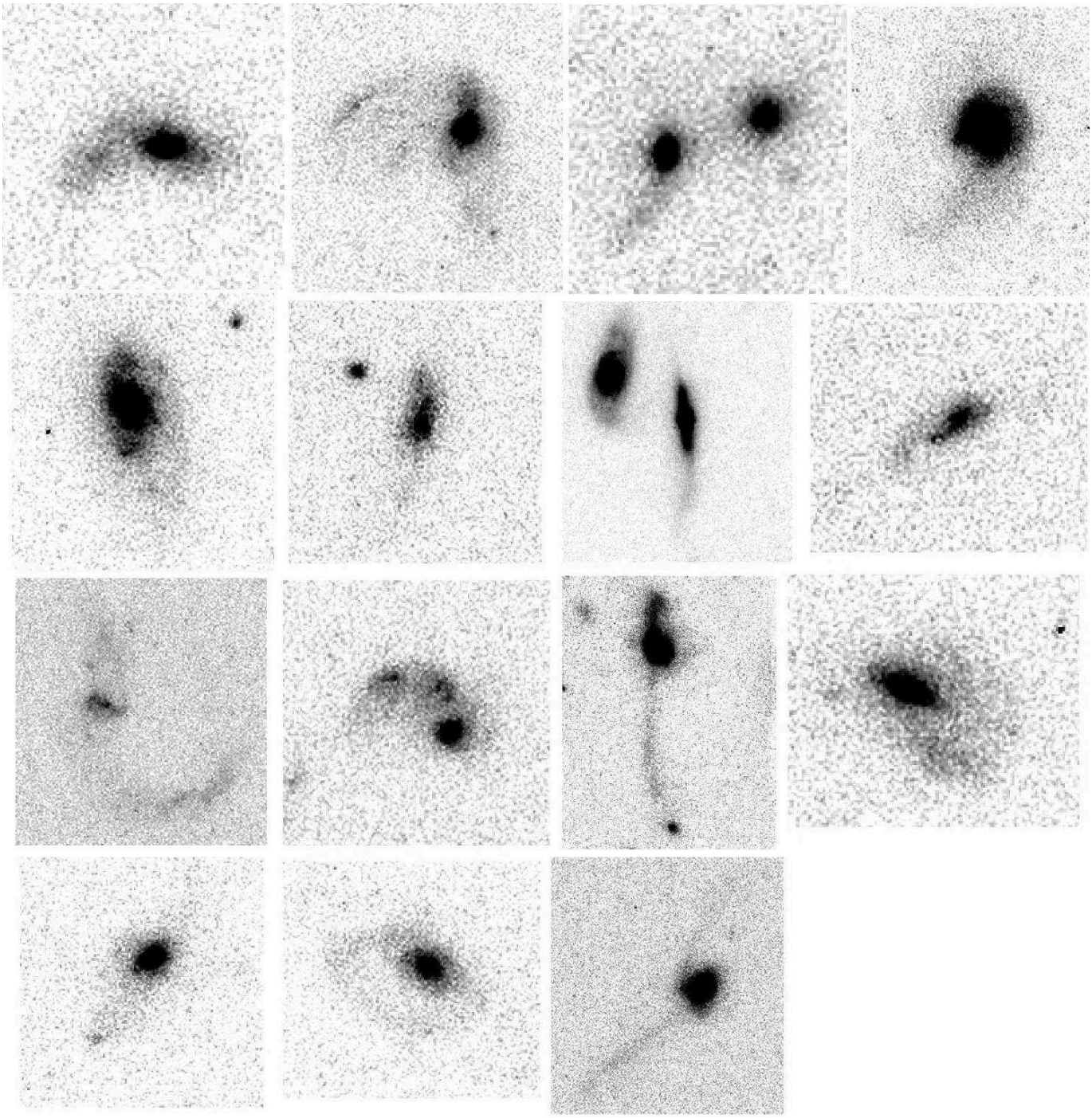

FIG. 2.— A sample of mergers with tidal tails in the ECDFS field. From left to right, galaxy IDs are 6494, 7357, 11072, 17207 (top), 20158, 24090, 29976, 30004 (the 2nd row), 30076, 44488, 45115, 57822 (the 3rd row), 57896, 60651, and 61546 (bottom).

finding extended tidal features that tend to have lower surface brightness at larger radii of the OHR of a galaxy. We point out that the total flux adopted here differs from that given, for example, in the Third Reference Catalogue of Bright Galaxies (RC3; de Vaucouleurs et al. 1991), where missing flux is added in by extrapolation of integrated luminosity profiles to infinite radius. This procedure is impractical for our analysis since we are not fitting light profiles. The measurements of A_o and D_o are nevertheless likely to be only marginally affected by this difference.

We test the A_o-D_o method for quantifying galaxy morphologies using our sample of 764 galaxies in comparison with the morphologies visually classified. Figure 3 illustrates the distribution of the sample in A_o-D_o diagram. Different morphological types are marked with different symbols. We can see that all sample galaxies lie on a tight sequence, where the location is in general correlated with the degree of morphological disturbance. Galaxies with stronger disturbed morphologies tend to have higher A_o and D_o. The vast majority of galaxies with regular morphologies (E, S0, Sa-b, Sc-d, edge-on disks) have $D_o < 0.5$ and $A_o < 0.6$, following a tight relation $\log A_o = 0.6 \log D_o$. This relation indicates that the two

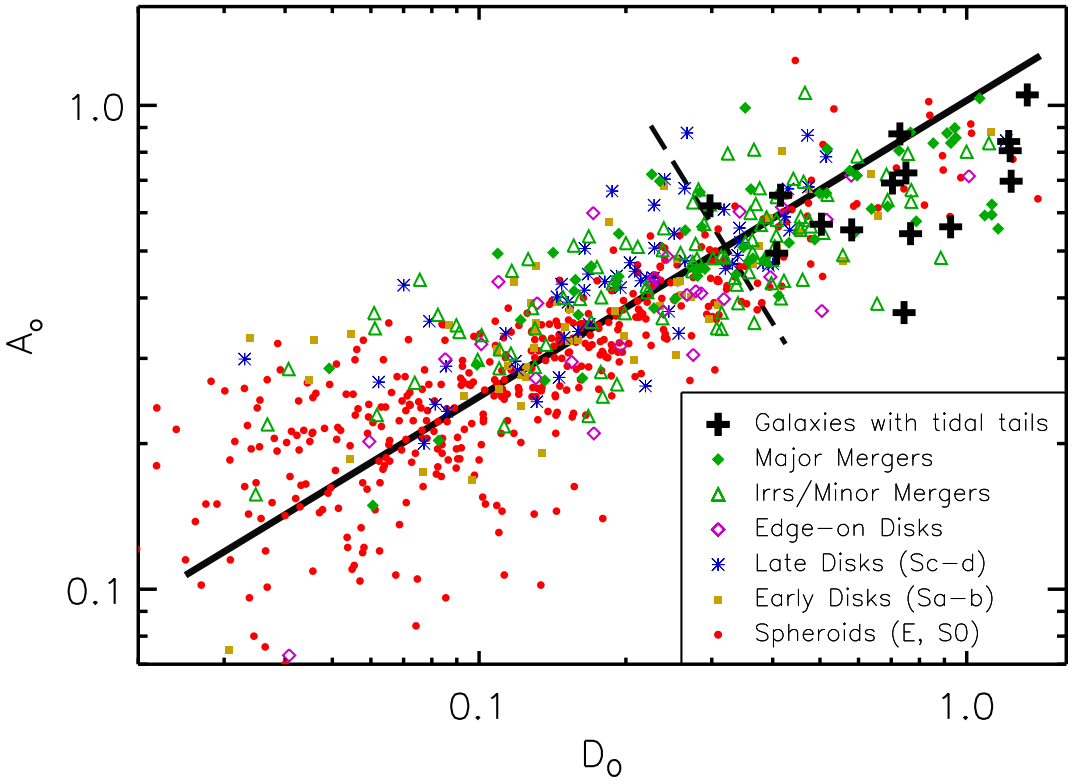

FIG. 3.— The A_o-D_o diagram of our sample of 764 galaxies with $\log(M/M_\odot) \geq 10.5$ and $0.35 < z < 0.9$ in the ECDFS. The two parameters are derived from *HST* z_{850}-band images, corresponding to the rest-frame optical for the redshift range examined here. The dashed line is the criterion for selecting tidal tails described as $\log A_o > -1.6 \log D_o - 1.1$. The solid line represents the sequence of regular galaxies best-fitted by $\log A_o = 0.6 \log D_o$.

parameters A_o and D_o are correlated with each other. This is also confirmed by the fact that no data points are found in the bottom-right and top-left regions of the diagram.

However, different morphological types of the sample galaxies are not clearly separated along the sequence. Spheroids and early disks having symmetric morphologies reside mostly in the region $D_o < 0.2$. Edge-on disks and late disks with non-symmetric substructures like arms, H II regions and stellar clusters are distributed more widely over the sequence. Such substructures are unlikely to be responsible for a high D_o. Irregular galaxies and major/minor mergers are systematically higher in A_o but spread over the full range of D_o.

The striking result from Figure 3 is that all galaxies with tidal tails (black crosses) have apparently higher D_o and higher A_o, compared with the galaxies of other morphological types, in particular regular ones (spheroids and disks). The large spread in D_o is mostly caused by the variety of the tidal tails in size and light weight relative to their host galaxies. The majority (12/15) of these with tidal tails are at $D_o > 0.5$. This indicates that D_o is sensitive to the tidal tails, although three objects with weak tidal tails (17207, 20158, 24090) have $D_o < 0.5$.

As shown in Figure 3, the criterion $\log A_o > -1.6 \log D_o - 1.1$ is sufficient to select all galaxies with tidal tails and most major mergers (32/60) in our sample. This cut, however, also picks up a large fraction (43%) of objects with irregular morphologies (irregulars/minor mergers). We note that some regular galaxies (spheroids and disks) also fall into the $D_o > 0.5$ region. We examined their images, and found that their A_o and D_o values are significantly affected by the unmasked residual light from neighboring sources. There are also 45 regular galaxies satisfying $\log A_o > -1.6 \log D_o - 1.1$ and $D_o < 0.5$. Again, we visually checked their *HST* images and segmentation maps. Of the 45 targets, 23 are contaminated by neighboring sources, and another 22 are isolated with asymmetric outskirts. Again the two morphological parameters A_o and D_o are largely overestimated for the visually-classified regular galaxies (spheroids and disks) due to the contamination. Figure 4 shows the 15 regular galaxies meeting the selection. We further investigate their morphological properties in detail for a better understanding of the selection.

Galaxy 49368: it has bright stellar clumps of 1 kpc size on one spiral arm, which seriously bias the estimation of A_o and D_o. Such features can be frequently seen in $z > 2$ disk galaxies. Minor mergers and instabilities in gas rich, turbulent disks are likely responsible for the formation of such clumps (Genzel et al. 2008; Bournaud & Elmegreen 2009; Dekel et al. 2009).

Galaxies 1032, 29488, 35796 and 61789: they are characterized by one prominent spiral arm. Their morphologies are similar to the so-called shrimp-type galaxies defined by Elmegreen et al. (2007). The highly curved spiral arm together with star-forming clumps on it usually imply that they are gas-rich systems disturbed by

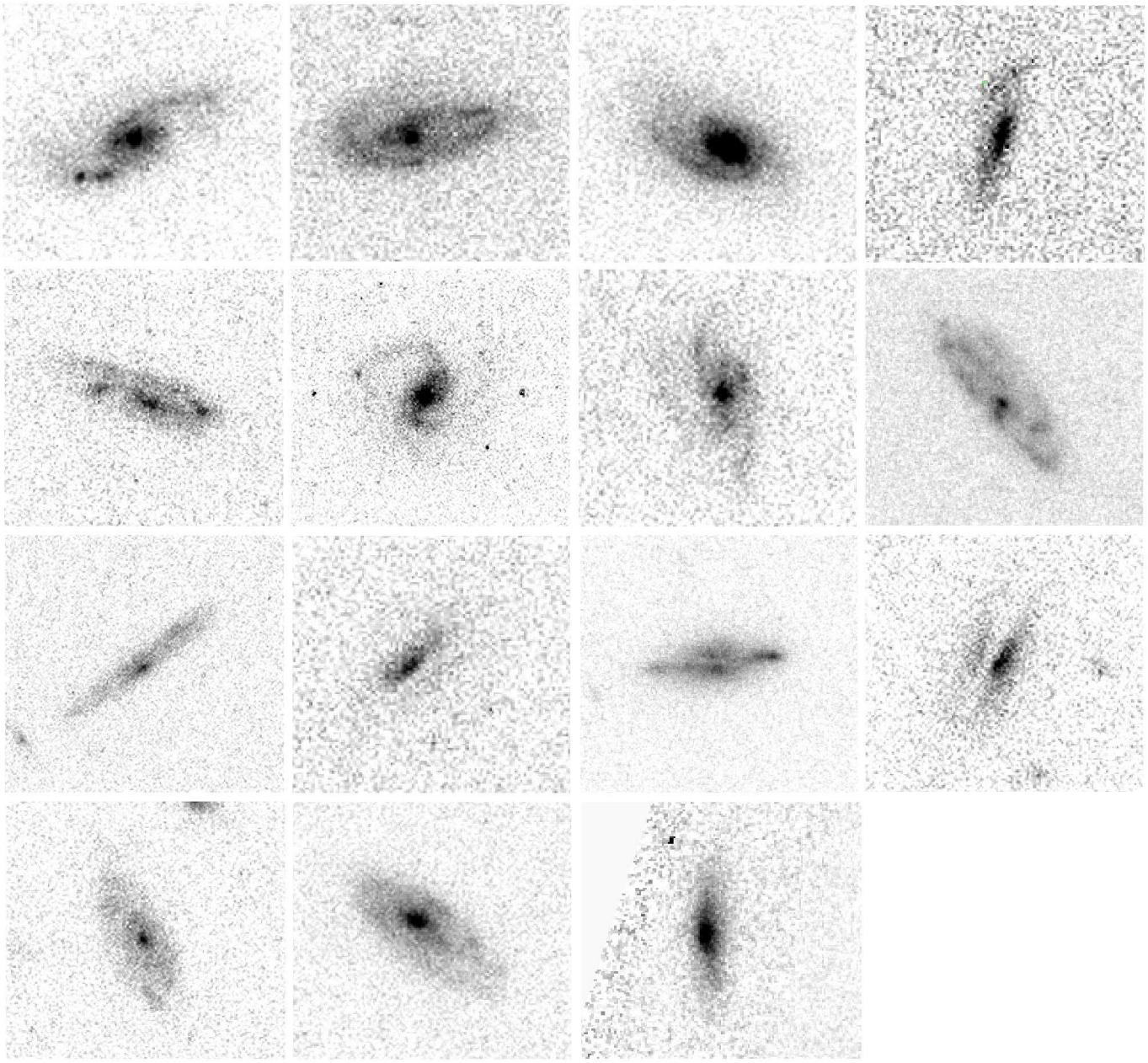

FIG. 4.— *HST* z_{850}-band images of sample galaxies satisfying the criterion $\log A_o > -1.6 \log D_o - 1.1$ and $D_o < 0.5$. These galaxies are visually classified as spheroids or disks. From left to right, the galaxy IDs are: 49368, 1032, 29488, 35796 (top); 61789, 2848, 42774, 42874 (the 2nd row); 20664, 30167, 30189, 56918 (the 3rd row); 37335, 59517, and 51329 (bottom).

minor mergers. However, no apparent signature is found for tidal disturbance in the four galaxies.

Galaxies 2848, 42774 and 42874: they have multiple spiral arms and show strong asymmetry in morphology.

Galaxies 20664, 30167, 30189 and 56918: they are edge-on disk galaxies with a clear dust lane feature. The dust lane divides the light profile of the parent galaxy into two parts. In such cases, the system is treated as a double core system in our analysis. The centroid of the IHR would significantly deviate from the geometric center if the dust lane is thick and splits the galaxy into two non-equal parts.

Galaxies 37335 and 59517: they are classified as Sd galaxies. Their surface brightness is relatively low. And their A_o and D_o are largely biased by clumpy light distribution and background noise.

Galaxy 51329: it is an edge-on disk galaxy. The disk is apparently warped. Minor mergers/interactions are often proposed as the cause of warped disks (Sanchez-Saavedra et al. 1990; Florido et al. 1991; Reshetnikov & Combes 1998; Ann & Park 2006).

It is worth noting that the segmentation strategy used in our analysis relies on a low detection threshold. This may potentially mistake some noise pixels for part of the target, resulting in a fuzzy appearance at edges. Since outer asymmetry and centroid deviation measure the morphological distribution of the OHR, the background noise may have noticeable effect

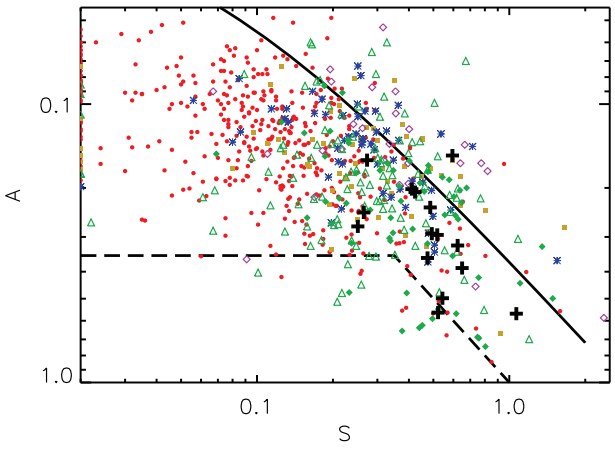

FIG. 5.— The relation between asymmetry (A) and clumpiness (S) for our sample. The solid line $A = 0.35S+0.02$ gives the relationship of nearby galaxies that are not involved in mergers while the dashed lines are the criteria ($A > 0.35, A > S$) for selecting merging galaxies (Conselice 2003). The data points are given in the same way as in Figure 3.

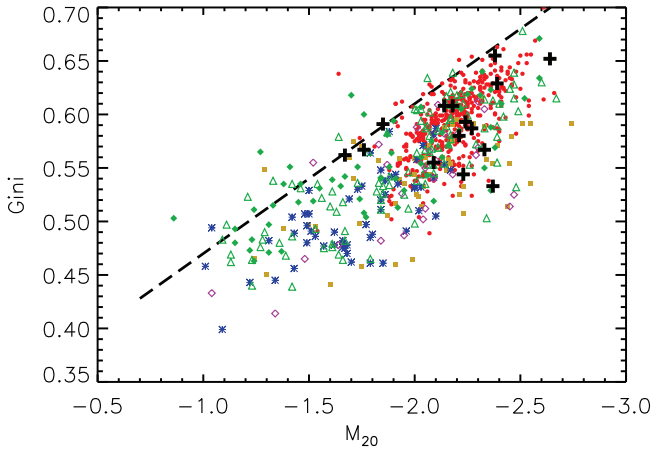

FIG. 6.— M_{20} versus Gini coefficient for our sample. The dashed line is the criterion ($G > -0.14\,M_{20} + 0.33$) from Lotz et al. (2004) for selecting merging galaxies. All symbols are given as same as in Figure 3. The majority of regular galaxies lie below the dashed line and form a well defined sequence.

on the estimate of the two parameters, in particular for low surface brightness galaxies.

Source deblending is also one issue that may affect the measurements of A_o and D_o. This is also key to extracting source catalogs from deep images. We adopted the optimal configuration for Sextractor from the GEMS catalog to produce segmentation maps for the selected sample galaxies. While the vast majority of sources can be properly resolved in the *HST* images with the configuration (see Caldwell et al. 2008 for more details), a small fraction ($<\sim$5%) of sources may still be contaminated by foreground or background sources due to projection effects, or over deblended into multiple sources. Merging galaxies with disturbed morphologies tend to suffer more from this problem. In this work, we visually examined the deblending for every sample galaxy and found a few cases with contamination by the neighboring sources which mislead the targets towards a high outer asymmetry.

4. COMPARISON WITH *CAS* AND GINI-M_{20}

The non-parametric methods *CAS* and Gini-M_{20} are widely used automatic approaches in the literature to identify merging galaxies. In this section, we compare our A_o-D_o method with the *CAS* and Gini-M_{20} methods in finding galaxies with extended tidal features.

4.1. *CAS*

The *CAS* method (Conselice et al. 2000; Conselice 2003) involves three morphological parameters: concentration (C), asymmetry (A) and clumpiness (or smoothness; S). The C parameter describes the intensity of stellar light contained within the central region in comparison to a larger outer region of a galaxy. The A quantifies the degree that the surface brightness profile of the galaxy deviates from a perfectly symmetric distribution. The S parameter focuses on the flux that is contained in the clumpy part of the light distribution. We calculate A and S parameters for our sample galaxies using *HST* z_{850}-band images. The results are shown in Figure 5. The solid line represents the $S-A$ relationship for regular galaxies in the local universe (Conselice 2003). It has been shown that the star formation activities lead to an increase in both S and A for nearby galaxies. We find, however, that our sample galaxies at intermediate redshifts deviate from the relationship of nearby galaxies. This has also been reported and explained in Conselice et al. (2008). The reason for such a deviation is that both S and A decrease when the resolution and signal-to-noise ratio (S/N) become lower. And S is affected by a larger degree than A.

In *CAS*, a galaxy is identified as a major merger when $A > 0.35$ and $A > S$. This selection works well for those where morphological distortion affects more than 35% of the total light of the galaxy. The condition $A > S$ ensures that the asymmetric light is not dominated by clumpy star-forming regions. Figure 5 shows that only about one quarter (16/60) of the major mergers (green diamonds) and one third (5/15) of galaxies with tidal tails (black crosses) in our sample satisfy $A > 0.35$. This is not surprising, as $A > 0.35$ statistically accounts for one third of the timescale for a major merger determined by N-body simulations, while minor mergers with mass ratio below 1 : 5 hardly reach $A > 0.35$ (Conselice 2006). This explains why only about one third of visually-classified major mergers and those with tidal tails in our sample are selected in Figure 5. We notice that some regular galaxies also show $A > 0.35$. It is mainly due to the contamination from neighboring sources within the target's 1.5 times Petrosian radius. A high A is obtained for galaxy 51329 due to the warped disk as shown in Figure 4.

We emphasize that our A_o parameter focuses on the morphological disturbance in the OHR of a galaxy in comparison with A that is dominated by the central high S/N light distribution and less sensitive to morphological disturbance in the OHR. It is clear that galaxies with tidal tails become largely indistinguishable from disks and irregular galaxies in Figure 5. Compared with Figure 3, we can conclude that our A_o-D_o method is more efficient than *CAS* in selecting galaxies with strongly disturbed morphologies like tidal tails.

4.2. *Gini-*M_{20}

The Gini coefficient (G) was originally invented in economics and introduced to describe the light distribution of a galaxy through a Lorentz curve (Abraham et al. 2003; Lotz et al. 2004). The Gini coefficient ranges from 0 to 1. A lower G means a more uniform flux distribution within a galaxy while a higher G means that a higher fraction of the total flux is contained in a smaller fraction of the galaxy pixels. M_{20} is a parameter to measure the second-order moment

of the light distribution of the top 20% brightest pixels in a galaxy which is then normalized to the light moment for all pixels. Like parameter C, it describes the central concentration of the brightest pixels of the galaxy depending on their distance from the galaxy center.

Figure 6 shows the distribution of our sample in the Gini-M_{20} diagram. We can see that our sample galaxies at intermediate redshifts are still distributed along a tight sequence following the nearby galaxies given in Lotz et al. (2004). The early-type galaxies have higher G and lower M_{20} (top-right) while late-type galaxies have lower G and higher M_{20} in a statistical sense. Lotz et al. (2004) suggested to select major mergers by the criterion $G > -0.14\,M_{20} + 0.33$ (the dashed line in Figure 6). However, there are only 9 of 56 major mergers (green diamonds) and one of 15 galaxies with tidal tails (black crosses) located above the dashed line. It has been pointed out that that mergers identified by the Gini-M_{20} method are not complete (e.g., Kampczyk et al. 2007; Scarlata et al. 2007; Kartaltepe et al. 2010). Simulations show that the Gini-M_{20} method primarily enables identifying mergers during the first pass or final stage when the galactic nuclei are distinguishable (Lotz et al. 2008, 2010a,b). The simulations also uncover that Gini-M_{20} is insensitive to mergers in the intermediate stage (i.e., maximal separation and/or second pass) when tidal tails may be formed. Comparison of Figure 6 with Figure 3 clearly demonstrates that our A_o-D_o method is better than Gini-M_{20} in identifying major mergers and galaxies with apparent extended tidal features.

5. DISCUSSION

Two parameters, outer asymmetry and centroid deviation, are developed to quantify the structure in the OHRs of galaxies, which usually have lower surface brightness than their IHRs. The tidal features like tidal tails in the OHRs are signatures of major mergers. Such delicate features are often extended and faint. Detecting low surface brightness emission in the OHRs is thus critical to the measurements of the two parameters.

We adopt a low threshold ($0.8\,\sigma_{\rm bkg}$) for source detection with SExtractor in order to probe the extended faint structures around a target. This may mis-identify some surrounding noise pixels as part of the target, yielding a fuzzy appearance although the contribution to the total flux is negligible (see Figure 1). The effect of noise on the structural properties in the OHR would become significant for low surface brightness galaxies. Such a detection technique based on surface brightness threshold has been widely used in studies of galaxy morphologies (e.g., Abraham et al. 2003). However, the physical size of detection of a given galaxy relies on the depth of the imaging and redshift due to the cosmological dimming effect. Then the detection completeness of tidal features needs to be addressed for the evolution of a population of galaxies with dedicated features. Law et al. (2007) adopted surface brightness threshold changing as $(1+z)^3$ to compensate for the cosmological dimming effect and ensure a constant surface brightness cut for all redshifts examined. This is beyond the scope of this work.

Alternatively, the elliptical or circular Petrosian radius (Petrosian 1976) derived from the growth curve of a galaxy can be used to determine the segmentation map of the galaxy. Taking the pixels within the Petrosian radius as the segmentation map is able to correct the cosmological dimming effect (Conselice 2003; Lotz et al. 2004). Nevertheless, this treatment may sacrifice the detection sensitivity of extended tidal features in the OHRs. For instance, the typical tidal tails of merging galaxies can be as extended as several tens of kpcs (Elmegreen et al. 2007) and beyond roughly 1$\sim$1.5 times Petrosian radius of the host galaxies.

Abraham et al. (2007) developed the so-called quasi-Petrosian segmentation method and claimed that it enables the probe of extended low surface brightness structures and the correction for the cosmological dimming effect. Firstly, all pixels of a galaxy in the SExtractor preliminary segmentation map are sorted in decreasing order of flux. The method will select pixels from the highest end of flux to the lowest end until a pixel meets $f_i = \eta(F_i/i)$, where f_i is flux of pixel i, and η is scale factor. F_i/i is the cumulative mean surface brightness. However, the fuzzy sky pixels will still be included when η is set lower for the detection of faint tidal tails.

6. CONCLUSION

We develop a new automatic method to quantify the structure in the outskirts of galaxies, aiming at probing delicate features like tidal tails. Using the isophote which encloses half the total light of a galaxy, the division of the galaxy image into two sections (the IHR and OHR) is the key to our method. Two parameters are introduced in the method: A_o, which measures the asymmetry of the OHR, and D_o, which measures the deviation of the intensity weighted centroids of the OHR from that of the IHR relative to the effective radius. The galaxies with stronger disturbance in morphology are expected to have higher A_o and D_o. Moreover, the two parameters are designed to be less affected by the central high surface brightness section of galaxies, and thus sensitive to low surface brightness features in the OHR. A sample of 764 galaxies with $\log(M/{\rm M}_\odot) > 3\times10^{10}$ and $0.35 < z < 0.9$ selected from the GEMS and GOODS-S surveys is used to verify our method. For a comparison, we visually classify morphologies for the sample using *HST* z_{850}-band images, following the usual classification scheme given in the literature. The z_{850} band corresponds to the rest-frame optical over the redshift range examined here.

Our investigation shows that all sample galaxies fall on a sequence in the A_o-D_o space. The position along the sequence is in general correlated with the degree of morphological disturbance. Galaxies with more disturbed morphologies have higher A_o and D_o in a statistical sense. The merging galaxies with tidal tails are well separated from regular galaxies (spheroids and disks) along the sequence. The regular galaxies are mostly with $D_o < 0.5$ and $A_o < 0.6$, following a relation described by $\log A_o = 0.6 \log D_o$. The galaxies with tidal tails are mostly with $A_o > 0.5$ and D_o ranging from 0.3 to 1.4. The criterion $\log A_o > -1.6 \log D_o - 1.1$ is able to select all galaxies with tidal tails and most major mergers (without apparent tidal tails).

The advantage of this selection is that major mergers with highly asymmetric morphologies are nearly complete and about 87% of galaxies with regular morphologies (spheroids and disks) are excluded at the same time. The left 13% of regular galaxies tend to have higher A_o and D_o contributed by odd spiral arms, strong dust lanes, warped disks, or contamination from neighboring sources. Low surface brightness galaxies suffer more from the contamination by surrounding sources or background noise, leaving A_o and D_o highly uncertain. Given that nearly 63% of the major mergers (including those with tidal tails) can be selected by a single cut in the A_o-D_o space, out method can be used for a relatively complete search for major mergers from large scale imaging surveys.

Compared with *CAS* and Gini-M_{20}, our A_o-D_o method is able to provide a better separation between mergers and regular galaxies. In particular, our method is unique in probing extended delicate features. In Gini-M_{20}, galaxies with tidal tails mix together with regular galaxies. And *CAS* is also insensitive to galaxies of this kind. We point out that our A_o is in a better position than *A* in *CAS* for probing asymmetric structures of galaxies.

Next-generation deep imaging surveys carried out by the Large Synoptic Survey Telescope (LSST) and Euclid will provide high-quality multi-band imaging data over large areas of sky, allowing for detailed studies of the structure and morphology of galaxies to address how galaxies form and evolve. Automatic approaches like our A_o-D_o method for morphological analysis are essential in the era of big data.

We are grateful to the referee for the helpful suggestions that improved this paper. We also thank Yinghe Zhao, Yewei Mao and Cong Ma for stimulating discussions. This work is supported by National Basic Research Program of China (973 Program 2013CB834900) and the Strategic Priority Research Program "The Emergence of Cosmological Structures" of the Chinese Academy of Sciences (Grant No. XDB09000000).

REFERENCES

Abraham, R. G., Tanvir, N. R., Santiago, B. X., et al. 1996, MNRAS, 279, L47
Abraham, R. G., Nair, P., McCarthy, P. J., et al. 2007, ApJ, 669, 184
Abraham, R. G., van den Bergh, S., & Nair, P. 2003, ApJ, 588, 218
Amendola, L., Appleby, S., Bacon, D., et al. 2013, Living Reviews in Relativity, 16, 6
Ann, H. B., & Park, J.-C. 2006, New Astronomy, 11, 293
Athanassoula, E., & Bosma, A. 1985, ARA&A, 23, 147
Barnes, J. E., & Hernquist, L. 1992, Nature, 360, 715
Barnes, J. E., & Hernquist, L. 1992, ARA&A, 30, 705
Bertin, E., & Arnouts, S. 1996, A&AS, 117, 393
Borch, A., Meisenheimer, K., Bell, E. F., et al. 2006, A&A, 453, 869
Bournaud, F., & Duc, P.-A. 2006, A&A, 456, 481
Bournaud, F., & Elmegreen, B. G. 2009, ApJ, 694, L158
Bridge, C. R., Carlberg, R. G., & Sullivan, M. 2010, ApJ, 709, 1067
Bundy, K., Fukugita, M., Ellis, R. S., Kodama, T., & Conselice, C. J. 2004, ApJ, 601, L123
Bundy, K., Fukugita, M., Ellis, R. S., et al. 2009, ApJ, 697, 1369
Caldwell, J. A. R., McIntosh, D. H., Rix, H.-W., et al. 2008, ApJS, 174, 136
Cardamone, C. N., van Dokkum, P. G., Urry, C. M., et al. 2010, ApJS, 189, 270
Carlberg, R. G., Cohen, J. G., Patton, D. R., et al. 2000, ApJ, 532, L1
Cassata, P., Cimatti, A., Franceschini, A., et al. 2005, MNRAS, 357, 903
Conselice, C. J. 2014, arXiv:1403.2783
Conselice, C. J. 2009, MNRAS, 399, L16
Conselice, C. J. 2006, ApJ, 638, 686
Conselice, C. J. 2003, ApJS, 147, 1
Conselice, C. J., Bershady, M. A., Dickinson, M., & Papovich, C. 2003, AJ, 126, 1183
Conselice, C. J., Bershady, M. A., & Jangren, A. 2000, ApJ, 529, 886
Conselice, C. J., Rajgor, S., & Myers, R. 2008, MNRAS, 386, 909
Conselice, C. J., Yang, C., & Bluck, A. F. L. 2009, MNRAS, 394, 1956
de Vaucouleurs, G., de Vaucouleurs, A., Corwin, H. G., Jr., Buta, R. J., Paturel, G., & Fouque, P. 1991, Third Reference Catalogue of Bright Galaxies (New York: Springer)
Dekel, A., Sari, R., & Ceverino, D. 2009, ApJ, 703, 785
Domingue, D. L., Xu, C. K., Jarrett, T. H., & Cheng, Y. 2009, ApJ, 695, 1559
Duc, P.-A. 2013, Astronomical Society of the Pacific Conference Series, 477, 47
Duc, P.-A., Bournaud, F., & Masset, F. 2004, A&A, 427, 803
Duc, P.-A., & Renaud, F. 2013, Lecture Notes in Physics, Berlin Springer Verlag, 861, 327
Elmegreen, B. G., Kaufman, M., & Thomasson, M. 1993, ApJ, 412, 90
Elmegreen, D. M., Elmegreen, B. G., Ferguson, T., & Mullan, B. 2007, ApJ, 663, 734
Florido, E., Prieto, M., Battaner, E., et al. 1991, A&A, 242, 301
Genzel, R., Burkert, A., Bouché, N., et al. 2008, ApJ, 687, 59
Giavalisco, M., Ferguson, H. C., Koekemoer, A. M., et al. 2004, ApJ, 600, L93
Häussler, B., McIntosh, D. H., Barden, M., et al. 2007, ApJS, 172, 615
Hibbard, J. E., & Mihos, J. C. 1995, AJ, 110, 140
Hopkins, P. F., Croton, D., Bundy, K., et al. 2010, ApJ, 724, 915
Hopkins, P. F., Hernquist, L., Cox, T. J., & Kereš, D. 2008, ApJS, 175, 356
Jogee, S., Miller, S. H., Penner, K., et al. 2009, ApJ, 697, 1971
Kampczyk, P., Lilly, S. J., Carollo, C. M., et al. 2007, ApJS, 172, 329
Kartaltepe, J. S., Sanders, D. B., Scoville, N. Z., et al. 2007, ApJS, 172, 320
Kartaltepe, J. S., Sanders, D. B., Le Floc'h, E., et al. 2010, ApJ, 721, 98
Kawata, D., Mulchaey, J. S., Gibson, B. K., & Sánchez-Blázquez, P. 2006, ApJ, 648, 969
Lacey, C., & Cole, S. 1993, MNRAS, 262, 627
Law, D. R., Steidel, C. C., Erb, D. K., et al. 2007, ApJ, 656, 1
Le Fèvre, O., Abraham, R., Lilly, S. J., et al. 2000, MNRAS, 311, 565
Lin, L., Patton, D. R., Koo, D. C., et al. 2008, ApJ, 681, 232
Lotz, J. M., Jonsson, P., Cox, T. J., et al. 2011, ApJ, 742, 103
Lotz, J. M., Jonsson, P., Cox, T. J., & Primack, J. R. 2010a, MNRAS, 404, 575
Lotz, J. M., Jonsson, P., Cox, T. J., & Primack, J. R. 2010b, MNRAS, 404, 590
Lotz, J. M., Jonsson, P., Cox, T. J., & Primack, J. R. 2008, MNRAS, 391, 1137
Lotz, J. M., Primack, J., & Madau, P. 2004, AJ, 128, 163
Man, A. W. S., Toft, S., Zirm, A. W., Wuyts, S., & van der Wel, A. 2012, ApJ, 744, 85
Mihos, J. C. 2004, Recycling Intergalactic and Interstellar Matter, 217, 390
Patton, D. R., & Atfield, J. E. 2008, ApJ, 685, 235
Patton, D. R., Pritchet, C. J., Carlberg, R. G., et al. 2002, ApJ, 565, 208
Patton, D. R., Pritchet, C. J., Yee, H. K. C., Ellingson, E., & Carlberg, R. G. 1997, ApJ, 475, 29
Petrosian, V. 1976, ApJ, 209, L1
Reshetnikov, V., & Combes, F. 1998, A&A, 337, 9
Rix, H.-W., Barden, M., Beckwith, S. V. W., et al. 2004, ApJS, 152, 163
Robaina, A. R., Bell, E. F., van der Wel, A., et al. 2010, ApJ, 719, 844
Sanchez-Saavedra, M. L., Battaner, E., & Florido, E. 1990, MNRAS, 246, 458
Sanders, D. B., & Mirabel, I. F. 1996, ARA&A, 34, 749
Scarlata, C., Carollo, C. M., Lilly, S., et al. 2007, ApJS, 172, 406
Springel, V., White, S. D. M., Jenkins, A., et al. 2005, Nature, 435, 629
Toomre, A., & Toomre, J. 1972, ApJ, 178, 623
Wetzstein, M., Naab, T., & Burkert, A. 2007, MNRAS, 375, 805
White, S. D. M., & Rees, M. J. 1978, MNRAS, 183, 341
Wright, A. E. 1972, MNRAS, 157, 309
Xu, C. K., Sun, Y. C., & He, X. T. 2004, ApJ, 603, L73
Xu, C. K., Domingue, D., Cheng, Y.-W., et al. 2010, ApJ, 713, 330